Emission measure analysis methods: the corona of AR Lacertae revisited

J.S. Kaastra[1], R. Mewe[1], D.A. Liedahl[2], K.P. Singh[3],[4], N.E. White[3], and S.A. Drake[3]

[1] SRON Laboratory for Space Research, Sorbonnelaan 2, 3584 CA Utrecht, The Netherlands
[2] V-Division, Lawrence Livermore National Laboratory, L-41, P.O. Box 808, Livermore, CA 94550
[3] Code 660, Laboratory for High Energy Astrophysics, NASA/GSFC, Greenbelt, MD 20771
[4] NRC Research Associate on leave from T.I.F.R., Bombay, India

Abstract. A simultaneous ROSAT/ASCA observation of the RS CVn binary AR Lac has been re-analysed using updated calculations for the plasma emission. Several analysis methods are applied that serve to reconstruct the emission measure distribution of AR Lac. In particular we describe the regularisation method, a Chebyshev polynomial method, a clean algorithm, a genetic algorithm and a method based upon broadened discrete temperature components. We confirm earlier results that the abundances are non-solar; for most elements (O, Mg, Si, S, Ar, Ca and Fe), we find abundances that are consistent with 1/3 of the solar photospheric abundances. The abundances of Ne (0.7) and Ni (1.1) are somewhat larger. The emission measure analysis shows that there are at least two and probably three temperature components: a cool, intermediate and hot component at temperatures of 0.6, 1 and 2.4 keV, respectively. The cool component is rather narrow (less than 50 % relative width) and there is no significant emission below 0.3 keV down to our detection limit at about 0.03 keV. The intermediate and hot component may be separate structures, but could also be the dominant features of a more continuous emission measure distribution between 1–4 keV. High-temperature emission above 5 keV is limited to at most 5 % of the total.

Key words: methods: data analysis – stars: abundances – stars: coronae – stars: individual: AR Lac – X-rays: stars

1. Introduction

X-ray spectra of stellar coronae contain important information on the temperature structure and abundances of these coronae. With the increased sensitivity and energy resolution of ASCA (Advanced Satellite for Cosmology and Astrophysics) it is now possible to study both the abundances and the temperature structure in more detail than has been possible before.

Send offprint requests to: J.S. Kaastra

A surprising result of observing several stars with the ASCA in the 0.4–10 keV band is that the elemental abundances are often very low when compared with those of the solar photosphere (White et al. 1994; Drake et al. 1994, 1996; White 1996). Similar results have also been found from observations with the Extreme Ultraviolet Explorer (EUVE) which samples the low energy (0.02–0.2 keV) end of the spectra (e.g., Stern et al. 1995; Rucinski et al. 1995).

The reality of these low abundances has often been disputed. In observations with the EUVE, the low abundances can be deduced from the relatively strong continuum in the 0.1 keV band, as compared to the spectral lines of iron. However, various alternative explanations for the low line-to-continuum ratio in the EUVE band have been given.

The first explanation is that a very high temperature (>1 keV) component, which, due to the high degree of ionisation of the plasma, produces a featureless continuum below 0.1 keV, with a nearly temperature-independent shape, can enhance the continuum relative to the line strengths. The energy bandwidth of EUVE is too limited to discard this possibility. A broader energy band can help to check the reality of a very hot component. As an example, simultaneous ASCA/EUVE observations of AB Dor (Mewe et al. 1996), yielded no evidence for a very hot component, but instead indicated that lower than solar abundances, in particular that of iron, cause the low line-to-continuum ratio.

Another explanation for the low line-to-continuum ratio is resonance scattering of some of the strongest EUV lines (Schrijver et al. 1994). This causes an effective intensity reduction of the strongest resonance lines. Resonance scattering possibly plays a role in Procyon and α Cen (Mewe et al. 1995a; Schrijver et al. 1995).

Alternatively, the EUV continuum at 0.1 keV may be due to a combination of many relatively weak but unresolved lines not included in the current plasma codes (Schmitt et al. 1996). In particular the line complexes due to L-shell ionisation of Ne, Mg, Si and S are possible candidates, since all of them occur at these energies.

X-ray observations in the 1–10 keV band with high spectral resolution contribute to the solution of this problem. For example, with ASCA the important K-shell lines of Si, S and Fe are all well separated, and the underlying bremsstrahlung and recombination continuum can be determined without doubt. Furthermore, resonance scattering appears to play no role in the ASCA X-ray band (see e.g., SWD), while the presence or absence of any component with a temperature above 1 keV can be easily established. Finally, the atomic parameters of the important Fe-L complex have been updated recently (Liedahl et al. 1995, Mewe et al. 1995b). This offers the opportunity to check the iron abundance as derived from both the K- and L- shell complexes.

Finally, a longstanding issue is whether the coronal temperature structure of stars is continuous, or whether it consists of discrete structures. Harrison & Thompson (1992) have compared previously existing methods for determining solar temperature distributions. Most methods described there are variants of the regularisation or polynomial methods described also in our paper. A major difference between their approach and ours is that they use a set of selected spectral lines, most of which are in the soft X-ray range, obtained from simulations of high-resolution spectroscopy of the sun, while we use real data with lower resolution, but utilising the complete spectrum (including continua) between 0.2–10 keV.

Here, we investigate these questions using simultaneous ASCA/ROSAT observations of AR Lac, which have been analysed before (White et al. 1994; Singh et al. 1996 (SWD hereafter)).

2. Observations

AR Lac is an RS CVn type eclipsing binary with an orbital period of 1.98 day at a distance of 50 pc and is one of the brightest coronal X-ray sources. It contains a G2 IV primary and a K0 IV secondary.

The present observations of AR Lac have been described in detail by Singh et al. (1996). We refer to that paper for more details. The simultaneous ROSAT and ASCA observations were taken from 1993 June 1–3. We used data from the ROSAT PSPC detector, and the SIS0 and GIS2 detectors of ASCA. The effective area of the SIS0 and GIS2 detectors were multiplied by 0.95 and 0.77 respectively, in order to match the ROSAT data (cf. SWD, Table 1a).

Our analysis differs from that of SWD in the following ways: Firstly, the rebinning scheme is slightly different. We rebinned the PSPC and GIS0 data to about 1/3 of the resolution (FWHM). However, we retained the requirement of having at least 20 counts per data channel, as was done by SWD. Regions with extremely low count rates at the low or high energy ends of the spectrum were omitted. We are left with 18 data channels for the PSPC (energy range 0.22–2.49 keV), 56 data channels for the GIS2 (energy range 0.80–8.30 keV), 154 data channels for the SIS0 (energy range 0.46–7.32 keV), thus in total 228 data channels. This has to be compared to the 594 data channels of SWD.

Secondly, we included a systematic error of 2 % of the source flux in all three data sets, in order to account for systematic errors in both the data and the spectral model. For the SIS0 data, there is additional uncertainty at lower energies; we have taken a systematic error of 5 % below 0.8 keV.

Thirdly, the energy grid on which the model spectrum is calculated is important. In our spectral model, the calculated flux is placed at the centers of the energy bins. The total spectrum is then convolved with the instrument response matrix. If the model energy bin width is ΔE, we make thus on average an rms error of $\Delta E/\sqrt{12}$ in the line center (the variance of a uniform probability distribution between 0–1 is 1/12). On the other hand, the line centroid can be estimated from the data with an accuracy of $\sigma/\sqrt{n}$ (apart from calibration errors), where σ is the gaussian width (σ =FWHM/2.35) of the instrument redistribution function, and n the total number of counts in the line. Clearly, the error introduced by the finite model bin width must be smaller than the statistical error on the line centroid. Thus, we have

$$\Delta E < 1.47\text{FWHM}/\sqrt{n} \ . \tag{1}$$

In our data set, the SIS0 data have the highest spectral resolution. The energy grid of the original SIS0 response matrix has a constant model bin size of 0.01 keV. The strongest lines in our spectrum have about 4000 counts. It appears that for the 20 strongest spectral lines in the data (derived from a first model fit), this binning of 0.01 keV is insufficient. Accordingly, we refined the energy grid near those lines to ΔE =0.001–0.005 keV.

3. Spectral model

For our spectral analysis, we have used the SPEX software package (Kaastra et al. 1995). This package contains models for the calculation of spectra from optically thin plasmas in collisional ionisation equilibrium (CIE) (Mewe et al. 1985, 1986; Kaastra & Mewe 1993). Recently the calculations for the Fe-L complexes have been updated using results from the HULLAC code (Liedahl et al. 1995; Mewe et al. 1995b). The differences between the newer calculations and the older versions of the code can be of the order of several tens of a percent with the resolution of the SIS of ASCA. Since the Fe-L complex dominates the spectrum near 1 keV, it is expected that the improved calculations could change the spectral fitting parameters drastically. We will in general express the derived coronal abundances relative to the solar photospheric values taken from Anders & Grevesse (1989) so as to facilitate comparisons with previous papers that have used these as the reference, except in Sect. 5.3, where we have adjusted them to the newer Grevesse et al. (1992) solar photospheric abundance values. For the ionisation balance we use Arnaud & Rothenflug (1985) for all elements except iron, for which we use the update of Arnaud & Raymond (1992). Emission measures Y are defined here as the integral over $n_e n_H dV$ where n_e is the electron density, n_H is the hydrogen density and V the emitting volume. Galactic absorption is taken into account using the model of Morrison & McCammon (1983).

4. Analysis

4.1. Two-temperature fits

As a first step we confirmed the results of SWD that fits with either a single temperature component or with two components with solar abundances did not give an acceptable fit: $\chi^2 = 1897$ for 215 degrees of freedom and $\chi^2 = 1536$ for 223 degrees of freedom, respectively.

Following SWD, we tried a fit with two CIE components with variable abundances for N, O, Ne, Mg, Si, S, Ar, Ca, Fe and Ni. The abundances of the other elements (He, C, Na and Al) were fixed at the solar values as our measurements are not sensitive enough to put useful constraints on the abundances of these elements. Initially we adopted the same abundances for both temperature components. The results are given in Table 1. Errors are based upon $\chi^2 + 2$ and correspond to 1σ errors (90 % confidence bounds are about 15 % larger). For comparison we also give the fit parameters as derived by SWD from the same observations but with an older version of the plasma code, without the improvement of the Fe-L complex, and for iron with the ionisation balance of Arnaud & Rothenflug (1985).

In general, our results agree well with those derived by SWD; the only significant differences appear to be the temperature of the cool component, for which we find a higher value, and some abundances: we find somewhat lower abundances for O, Fe, Ne and Mg. These differences can be easily understood. Fig. 10 of Arnaud & Raymond shows that for the same charge state of iron, the corresponding temperature increases by 20 % and 10 % for the cool and hot component respectively, if the ionisation balance of Arnaud & Rothenflug (1985) is replaced by that of Arnaud & Raymond (1992). This is indeed what we did as compared to SWD. The true temperature increase is, however, slightly smaller: 11 % and 1 % respectively. This is smaller than what is expected from iron alone, because the ionisation balance for the other elements that play a role in the temperature determination has not been changed. Our smaller iron abundance can be explained by the small increase in Fe-L emissivity in our newer plasma code as compared to the code used by SWD; we need less iron in order to explain the same line flux. Since the important neon and magnesium lines are surrounded by strong Fe-L lines, a decrease in the Ne abundance is not surprising.

4.2. Three-temperature fits

We also investigated the possibility that there is a third significant temperature component in AR Lac. Our instruments are sensitive for temperatures in the range of about 0.03–10 keV. We have searched this temperature range and checked for each temperature to see how the fit improves by adding an extra temperature component.

We derive an upper limit of $0.60\ 10^{59}$ m^{-3} for the emission measure of any temperature component in the 0.05–0.4 keV temperature range, i.e. less than 5 % of the total emission measure of the cool and hot component. If the third component is very hot ($T > 4$ keV), we find an upper limit for the emission measure of $0.5\ 10^{59}$ m^{-3}, i.e. also no more than 5 % of the total.
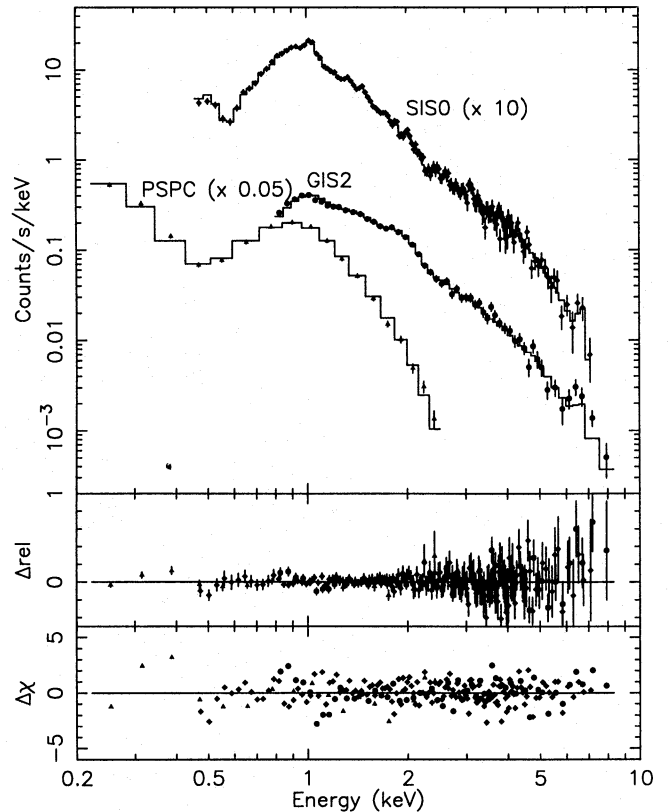

Fig. 1. AR Lac spectrum with best fit three-temperature model. Triangles: ROSAT PSPC data; diamonds: ASCA SIS0 data; circles: ASCA GIS2 data. Upper panel: observed spectrum with best fit model (solid histogram). For clarity of representation, the PSPC data have been multiplied by 0.05 and the SIS0 data by 10. Middle panel: relative fit residuals Δrel: (observed - model) / model. Lower panel: fit residuals $\Delta\chi$: (observed - model) / error.

We did, however, find a significant improvement by adding a third, intermediate temperature component near 1 keV. Fig. 1 shows our best fit spectrum. The fit is acceptable at the 10 % confidence level. The count rates of all spectral bins are within 3σ from the model. The only significant ~15 % fit residuals appear to be in the PSPC data below 0.4 keV and the SIS0 data below 0.53 keV. The calibration of both the instruments is known to be somewhat inaccurate at these low energy ends of the bandwidth.

There also appears to be a slight deficit of the model near the Fe-K complex above 6 keV, especially in the GIS2 data. This motivated us to try a fit with the iron abundances of all three components decoupled. The fit did not improve significantly: $\Delta\chi^2 = 3.4$ for 2 additional free parameters, although the fit residuals above 6 keV are indeed smaller. The improvement is made by shifting the intermediate temperature component from 1.1 to 1.4 keV and the hot component from 2.4 to 4.3 keV; the best-fit abundances for the cool, intermediate and hot component are 0.25, 0.15 and 0.42 respectively, although within their respective error bars they are consistent with the average abundance of 0.22. In any case, our conclusion of a non-solar

Table 1. Three temperature fit parameters

Parameter	3 comp present work	2 comp present work	2 comp SWD
χ^2	238.8	254.1	770.9
dof	211	213	577
N_H (10^{22} m^{-2})	< 2.2	< 1.9	<4.4
kT_1 (keV)	0.61±0.47	0.652±0.016	0.586±0.015
kT_2 (keV)	$1.09^{+.23}_{-.12}$	-	-
kT_3 (keV)	$2.40^{+.56}_{-.24}$	2.01±0.07	1.98±0.06
Y_1 (10^{59} m^{-3})	3.73±0.78	5.06±0.38	4.14±0.27
Y_2 (10^{59} m^{-3})	3.33±0.99	-	-
Y_3 (10^{59} m^{-3})	4.25±1.27	6.13±0.29	6.25±0.24
Abundances:			
N	< 0.13	< 0.15	< 0.15
O	0.26±0.06	0.28±0.06	0.41±0.05
Ne	0.70±0.17	1.04±0.12	1.42±0.13
Mg	0.35±0.06	0.36±0.06	0.50±0.07
Si	0.31±0.04	0.30±0.05	0.40±0.06
S	0.17±0.07	0.15±0.07	0.19±0.09
Ar	0.35±0.26	0.30±0.23	0.31±0.27
Ca	< 0.34	< 0.31	< 0.25
Fe	0.22±0.02	0.19±0.02	0.29±0.03
Ni	1.06±0.32	1.43±0.32	1.14±0.36

iron abundance remains firm, even if the three components have different abundances.

Alternatively, we fixed the ratio of the metal abundances with respect to iron to the ratios implied by Table 1, but allowed the iron abundance and hence the global metallicity of the three components to be different. The χ^2 of the fit then improves marginally with 5.3, for 2 additional free parameters; the derived temperatures and emission measures are consistent with the values of Table 1. We find best fit metallicities corresponding to an iron abundance of 0.23(-0.07,+0.15), 0.17(-0.05,+0.18) and 0.36±0.10 for the cool, intermediate and hot component respectively. Since we cannot constrain iron abundance differences among the components with sufficient confidence, we adopted the same abundances for all the temperature components in the subsequent analysis.

We have also investigated the possible role of the electron density. In particular the He-like triplets are density sensitive. A fit with a free electron density, however, gave no significant improvement in the χ^2 with $\Delta\chi^2$ less than 2. We could not derive any interesting limit on the density. This is mainly due to the fact that ASCA is not able to resolve the He-like triplets of the important elements.

4.3. Continuous emission measure distributions

An unanswered question for many years has been the nature of stellar coronal temperature distributions: are they discrete or continuous? In order to investigate this, we have developed several methods to analyse the emission measure distribution with continuous models. All methods are based on a pre-calculated set of model spectra $F_i(E)$ for a temperature grid T_i. These model spectra take into account the appropriate abundances, interstellar absorption and are folded through the instrument profile. The emission measures Y_i for the temperature grid must be determined by matching the observed spectrum $S(E)$ as good as possible to the model spectrum

$$F(E) = \sum_i Y_i F_i(E) . \tag{2}$$

A given emission line is formed in a temperature range spanning typically ~ 0.3 in $\log T$. Thus a logarithmic temperature grid with a binning of 0.1 in $\log T$ is sufficient to derive the temperature distribution. Our instruments are sensitive for temperatures in the range of about 0.03–10 keV. Thus we limit the temperature grid to this range, yielding 26 bins for $\log T(\text{keV})$ ranging from -1.5–1.

Below we discuss various analysis methods: the regularisation method, the polynomial method, a clean algorithm, a genetic algorithm and finally a model based upon broad discrete components. The first two methods are oriented towards smooth temperature distributions. All of these methods are now incorporated in our spectral analysis code SPEX. We apply them here to the present AR Lac spectrum. None of these methods gives acceptable fits for a spectrum with solar abundances. We, therefore, restrict our discussion to solutions with abundances as found from our three-temperature fit. Note that SWD treated the abundances as free parameters in the continous distribution models. The number of free parameters in each of these methods is in general the number of temperature bins used for the regularisation, clean and genetic methods; the order of the polynomial used in the polynomial method and three times the number of components for the broad multi-temperature method.

4.3.1. Regularisation method

The first method we discuss is treated in more detail by Mewe et al. (1995a) and Schrijver et al. (1995). In brief, this method uses direct matrix inversion of Eq. (2) with the additional constraint that the second order derivative of the solution Y_i with respect to the temperature is as smooth as possible. This is done in order to damp unphysical oscillations otherwise present in the solution. The degree of smoothing is controlled by the regularisation parameter R, which is essentially a measure of the relative weight of the smoothness constraint with respect to the χ^2-minimisation constraint. The parameter R must be adjusted by hand or using statistical arguments. $R = 0$ corresponds to no smoothing at all. In general, it can be argued that the optimal R must be chosen such that

$$\chi^2(R) = \chi^2(R=0) \left(1 + f \sqrt{\frac{2}{n_{\text{channel}} - n_T}} \right) , \tag{3}$$

where n_{channel} is the number of data bins, n_T the number of temperature bins, and f a factor of order unity. $n_{\text{channel}} - n_T$ is the number of degrees of freedom of the fit; the argument is based on the fact that the mean and variance of a stochastic

Table 2. Regularisation method

R	χ^2	p	f
0.00	212.0	11.1	0.00
0.02	225.7	10.2	0.65
0.20	229.1	21.3	0.81
2.00	239.3	11.2	1.29

Fig. 2. Emission measure distribution of AR Lac obtained with the regularisation method. Dashed line: $R = 0.02$. Crosses: $R = 0.20$. Dotted line: $R = 2.0$

variable which has a χ^2 distribution with n degrees of freedom are n and $2n$ respectively.

The regularisation method works optimally for smooth, continuous temperature distributions. However, simulations show that it can also find discrete temperature structures, although it cannot resolve them to better than a factor of ~ 2.

A drawback of the regularisation method is that it cannot prevent the solution from taking negative values at some temperatures. However, it is possible to estimate the uncertainty ΔY_i on Y_i, and a solution is acceptable if not too many Y_i's are significantly below zero. In fact, it can be shown that in the worst case of no signal in the data, the expected number of negative Y_i values is half the number of temperature bins. We develop a criterion to weigh how much positiveness is violated, by defining the "penalty" p as

$$p \equiv \sum_{Y_i < 0} (Y_i/\Delta Y_i)^2 \ . \tag{4}$$

For a zero signal, the expected value for p is $n_T/2$ and its standard deviation is of the order of $\sqrt{n_T}$. For positive spectra p should be typically smaller than this. Very large values of p (possibly in combination with a large χ^2 value) could indicate problems with the model used (e.g., wrong abundances) or systematic errors in the data.

At the low and high temperature end of the grid, the spectrum is often not sensitive to the precise temperature value; it is then only possible to state that there is some very soft or hard spectral component, without being able to specify the precise shape of the corresponding temperature distribution. This should be remembered when investigating for example hard "tails".

In Fig. 2 we show our solution for three values of the regularisation parameter R (see also Table 2). These solutions are all acceptable (cf. Eq. (3)). The penalty p is somewhat too large for $R = 0.2$, mainly due to a negative "tail" below 0.06 keV. However the ROSAT PSPC is not very sensitive to spectral variations at temperatures near or below 0.1 keV, and this structure should not be regarded as realistic. Its negative flux contribution is partly compensated for by the small peak near 0.1 keV, which therefore should be interpreted cautiously, because it is also influenced by the minor negative excursion between 0.2–0.3 keV. Fig. 2 shows a bigger negative tail for $R = 0.02$ as compared to $R = 0.2$, but p is smaller due to larger error bars on the emission measure. χ^2 is somewhat better than our three-temperature fit (which has $\chi^2 = 238.8$), but one can argue that in fact a better measure of the goodness-of-fit of the regularised spectrum
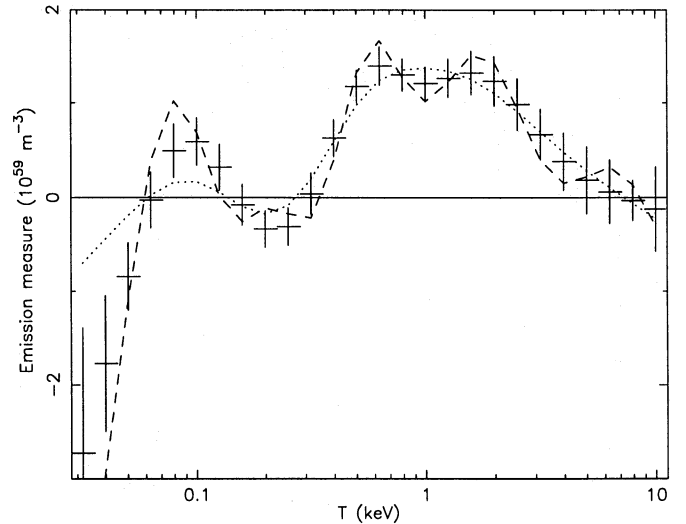
would be the sum of χ^2 and p. If we take that measure, our fit is not significantly better than the three-component fit.

The most important feature of our fit is the broad component between 0.4–3 keV, which shows an indication for two subcomponents at 0.6 and 2 keV, corresponding nicely with the cool and hot component of our three-temperature fit. There is no indication for the presence of very hot plasma ($T > 5$ keV). The total emission measure between 0.4–6 keV of $11.8 \ 10^{59}$ m^{-3} agrees well with the total emission measure of the three temperature components ($11.3 \ 10^{59}$ m^{-3}).

4.3.2. Polynomial method

A second method that is useful for smooth emission measure distributions is the polynomial method. This method has been applied before to EXOSAT data (Lemen et al. 1989) and EUVE data (Stern et al. 1995). We implemented this method here by writing the logarithm of the emission measure as the sum of n Chebyshev polynomials, that are a function of the logarithm of the temperature. This ensures that the emission measure distribution is positive for all temperatures, and that low and high temperatures have the same relative resolution.

By increasing the number of coefficients, the fit improves in general significantly, up to n about 8–10. For larger values of n, the χ^2 of the fit does not improve significantly. We found χ^2 values of 238.6–238.9 for n between 8–10, i.e. nearly the same as for our three-temperature fit. In Fig. 3 we show the corresponding emission measure distributions. All solutions have a double-peaked structure, corresponding to the cool and hot component at 0.6 and 2 keV respectively. There is an indication for emission between those components.

There could be a very weak high-temperature tail above 3 keV, but all 3 solutions presented here differ considerably in this region: e.g. $n = 8$ has no tail, $n = 9$ has an extended tail up to 8 keV while $n = 10$ has only a small peak near 6 keV. Thus
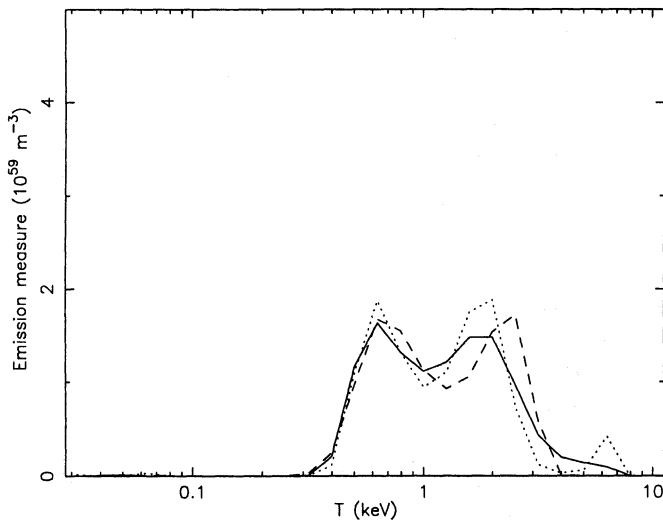
Fig. 3. Emission measure distribution of AR Lac obtained with the polynomial method. Dashed line: $n = 8$. Solid line: $n = 9$. Dotted line: $n = 10$.
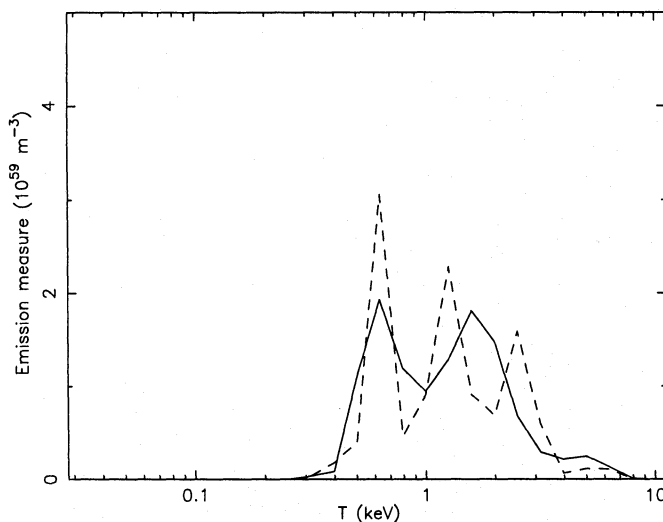

Fig. 4. Emission measure distribution of AR Lac obtained with the polynomial method using a narrower temperature grid (0.3–10 keV). Solid line: $n = 9$. Dashed line: $n = 13$.

a high temperature tail, if present at all, is weak but the details are uncertain.

Below 0.6 keV, the emission measure drops rapidly to zero near 0.4 keV. There is no indication for a significant emission component below 0.3 keV. Since the typical resolution in $\log T$ is the temperature range divided by n (about 0.2–0.3 in our case), we also tried some fits in the constrained temperature range 0.3–10 keV. We get essentially the same χ^2 values as for the broader temperature grid. Fig. 4 shows 2 typical solutions. For $n = 9$ (resolution ~ 0.17 in $\log T$) the solution is similar to our previous result, except that the two main temperature peaks are sharper. For $n = 13$, we recover a three-temperature structure with dominant temperatures in agreement to our three-

temperature fit. Since the χ^2 values of both these fits differ by no more than 0.2, it is not possible to discriminate between both models. The fit with $n = 9$ appears to have averaged the intermediate and hot component, and probably needs a weak high temperature tail in order to model the highest energy part of the spectrum correctly.

Note: SWD report that the fitting routine for the Chebyshev polynomial used in their paper was found to contain a bug that forced the emission measure distribution to be of continuously rising type. Using the new VMEKAL code (essentially the same plasma code as used here) and the corrected Chebyshev polynomial routine (order 6) which does not depend on the exponential of the polynomials, they found that the best-fit solution has a a double peaked distribution with maxima near 1 keV and 5 keV and a χ^2 that is not significantly different from that obtained from their 2T model. However the solution becomes negative at high temperatures. In the present analysis this is prohibited because we fit the logarithm of the emission measure distribution. The best-fit values for the abundances are similar to that in the 3T model presented here (Table 1).

4.3.3. Clean algorithm

The clean algorithm (Högbom 1974) is a powerful tool developed originally for the analysis of radio interferometer data. We have implemented it as follows. The observed spectrum $S(E)$ is correlated with our model spectra $F_i(E)$. The temperature T_j which shows the highest correlation coefficient is most likely the dominant contributor. We determine the best fitting emission measure Y_j for this temperature. In principle, if the source spectrum would be really a single temperature spectrum, this would be our final solution. We could subtract the corresponding model spectrum $Y_j F_j(E)$ from the observed spectrum $S(E)$ and would be left with noise only. However due to the presence of other temperature components, the best fit emission measure Y_j does not correspond to the true emission measure at that temperature, but is merely an order-of-magnitude estimate. Accordingly, we subtract only a small fraction (1 %) of this model component from the observed spectrum (we replace $S(E)$ by $S(E) - 0.01 Y_j F_j(E)$). We also put the corresponding emission measure $0.01 Y_j$ in our target solution vector. Using the corrected spectrum, we repeat the steps taken before by again determining the temperature with the best correlation. This might be the same as before, but could now also be another temperature. The process is repeated as long as the corresponding χ^2 is decreasing. If the solution has converged, we are left with only the noise in the observed spectrum, and the total emission measure distribution in our target solution vector.

Our simulations show that this method is very fast and powerful for discrete temperature structures. It is very well suited for reconstructing single, double or multi-temperature structures. For continuous temperature distributions it tends to make the solution somewhat "spiky", due to the subtraction of discrete components; however the average value of the solution over a somewhat broader temperature range (typically a factor 0.3 in $\log T$) is in good agreement with the average value of the input model.
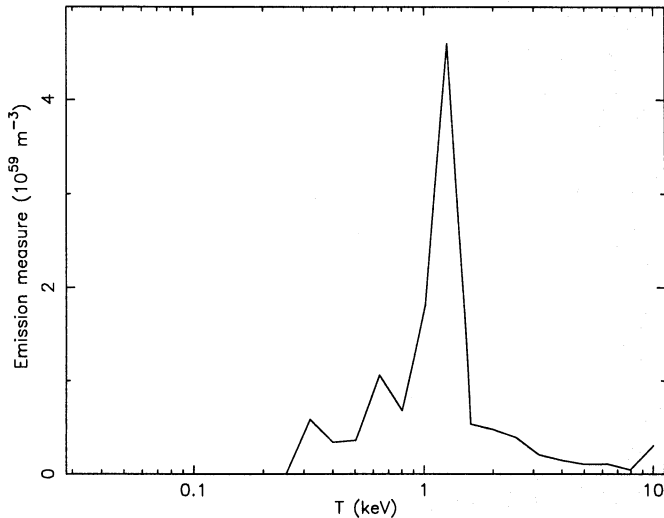
Fig. 5. Emission measure distribution of AR Lac obtained with the clean method.

Application of the clean method to the present AR Lac data did not result in an acceptable fit: $\chi^2 = 419$. The corresponding emission measure distribution is shown in Fig. 5. The bad fit is somewhat surprising, given the fact that for other sources we obtained good results with this method. The reason for the failure in this case is the following. At the beginning of the process, the highest correlation is found for a temperature of about 1 keV. Thus, the algorithm starts subtracting model flux at this temperature. This can be seen also in Fig. 5, where a dominant 1 keV component is present. Only later the other temperature components become evident, in particular the cool component at 0.6 keV is visible. Unfortunately the algorithm cannot correct the over-estimated 1 keV component sufficiently, leading to a fit that is not acceptable.

Why is the correlation coefficient of the observed spectrum with a 1 keV temperature plasma so high, in fact higher than for either a 0.6 keV or 2 keV plasma, despite the fact that these two appear to be the dominant components in AR Lac? The reason is that a plasma of 1 keV looks rather similar to a linear combination of a 0.6 keV and a 2 keV plasma, at least with the resolution and sensitivity of our instruments. In the part of the spectrum with the highest signal-to-noise ratio, a linear combination of the cool and hot component deviates no more than 10–20 % from a 1 keV plasma. Of course, the temperatures of 0.6 and 2 keV differ no more than a factor of 0.3 in $\log T$ from 1 keV, close to the resolution limit for the clean method mentioned above.

Despite this, our solutution does show that there is no emission below 0.3 keV, and again there is a hint of a weak high-temperature tail.

4.3.4. Genetic algorithm

We have also estimated the temperature distribution by using a genetic algorithm (Charbonneau 1995). Genetic algorithms are based on the biological notion of evolution by means of natural selection. They use an initial population of randomly chosen solutions. Each solution is assigned a fitness. By breeding this population, using crossover and mutation of the genes of the individuals, the population gradually evolves towards a solution with higher fitness. For more details we refer to the paper of Charbonneau, from which we have used the fortran code.

In our implementation, an individual of the population corresponds to a DEM distribution. The "genes" of each individual consist of the values of the emission measure at the given temperature grid. For the fitness of an individual we take minus the χ^2-statistic of the corresponding model spectrum as compared to the observed spectrum; thus increasing fitness means decreasing χ^2. We take an initial population of 1024 individuals. This is larger than recommended by Charbonneau, but we have chosen this because the number of parameters to be fit is large. The temperature grid is the same as for the other DEM methods (26 bins logarithmically spaced between $0.03 - 10$ keV).

The following settings in the implementation of Charbonneau are used. We use steady-state-replace-worst reproduction (i.e. each time a new individual is bred, it replaces the individual in the population with the worst fitness, but only if the new individual has a better fitness). We use elitism (i.e. the fittest individual is never deleted from the population). Fitter individuals have a higher breeding probability than others according to their ranking on a fitness scale. The crossover probability is 0.85, the initial mutation rate 0.005, the maximum mutation rate 0.25. The mutation rate increases in 10 generations to its maximum value. For the AR Lac spectrum, the initial median χ^2 value of the first generation is typically 5000; within about 10 generations the median fitness of the population evolves to about 500. After that, convergence is only slow, and improvements result in general mostly from mutations rather than crossover at these later generations.

In order to speed-up convergence, it is important to constrain the possible parameter space as much as possible. We have done this by demanding that the solution at each temperature must be smaller than some maximum Y_{max}. This maximum is determined for each temperature from the following condition: the sum of the squares of the fit residuals for those data channels only where $Y_{max}F_i(E) > S(E)$, should not exceed $n_{channel}/2$. Here $n_{channel}$ is the number of data bins. For Charbonneau's algorithm, the parameters (genes) must be scaled to the (0–1) interval. In principle, a scaling $Y = xY_{max}$ with x in the [0–1] interval would appear logical. However, we had more success with the following semi-empirical scaling:

$$Y = Y_{max}10^{4(x^{20} - 1)} . \tag{5}$$

This transformation favors the occurrence of genes with small emission measures; it does make the initial population resemble more to a single-temperature population. Further, the convergence improved by renormalising each solution by a single scale factor in order to minimise χ^2.

Finally, during our initial tests, it appeared that near convergence the solution sometimes "flipped" a temperature component by distributing part of its flux over the two neighbouring bins. This reflects the fact that for sufficiently fine temperature
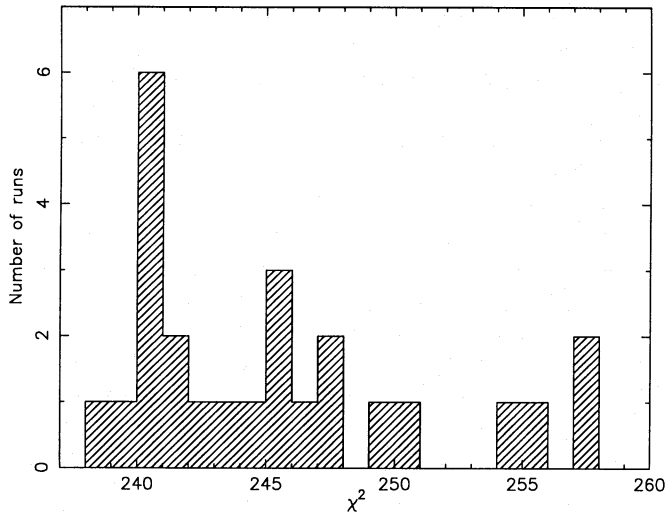
Fig. 6. Distribution of χ^2 for 25 runs with the genetic algorithm.
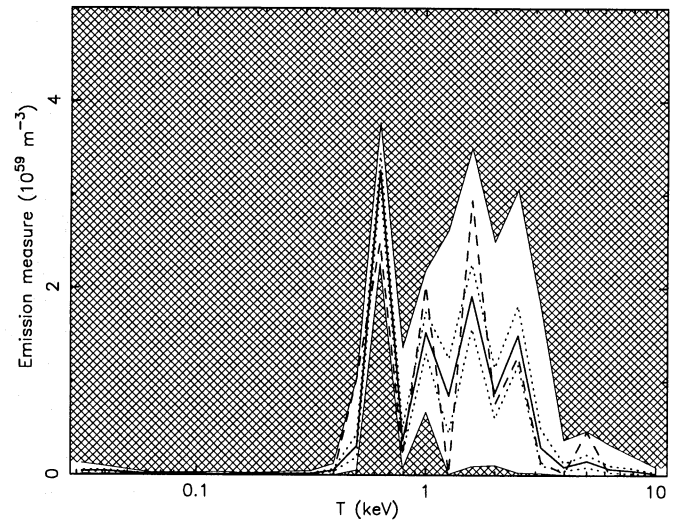

Fig. 7. Emission measure distribution of AR Lac obtained with the genetic algorithm, based on the 10 best solutions out of 25 runs. The average emission measure of these 10 soulutions (solid line) and its 1σ error bounds (dotted lines) is shown, as well as the emission measure of the best solution (dashed line). The region excluded by all 10 solutions is hatched.

binning, the spectrum at a certain temperature is approximately a linear combination of the spectrum at the neighbouring bins. In the later generations of our runs, mutations are important. Unfortunately, it is rather difficult to do these "flippings" with mutations, since it requires that at the same time that the emission measure of the relevant temperature bin mutates, the emission measures of the two neighbouring bins mutate in a consistent way. We resolved this by adding redundancy in the genes. For each temperature, we define three genes: the first gene is the total emission measure for the bin and its two neighbouring bins, scaled according to Eq. (5), the second is the fraction of the total emission measure of these three bins in the central component, and the third is the fraction of the remaining flux that is in the lower temperature bin of the three. Thus, "flippings" of emission measure can occur by only a single mutation in the second gene. The total emission measure at a certain temperature is then determined from the relevant contributions in three bins.

Further, the convergence improved by initially making a run of only 10 generations. For this population, we determined for each temperature the best value Y_b, as well as the maximum deviation Δ_Y from this best value. We then used the maximum of $1.2Y_b$ and $Y_b + 1.5\Delta_Y$ as a new constraint for the allowed emission measure range. Using this tighter, empirical constraint, we then did a final run with 200 generations. The advantage of this procedure is that our final run starts with a population that has on average a much lower χ^2 than the initial population of the first run, thus allowing a better convergence.

We have made 25 different runs. The spread in final χ^2 values is shown in Fig. 6. The plot shows a sharp peak of solutions with χ^2 close to 240, with an extended tail up to ~ 260. Clearly, the solutions in this tail are not completely converged. The solutions in the peak all have χ^2 values that are comparable to our best fit three-temperature model, as well as to the polynomial method. Therefore, we argue that the solutions in this peak are converged towards the absolute minimum (within an insignificant spread of about 2 in χ^2).

In Fig. 7 we plot the emission measure distribution for the best 10 solutions, all of which have χ^2 values between 239.0–241.8, as well as the maximum and minimum value they attain at any temperature. Also the best solution (χ^2=239.0) is shown. All solutions show the absence of significant emission components below 0.3 keV down to our limit at $\sim$0.03 keV. The cool component at 0.6 keV is narrow and present in all solutions. Its strength differs by no more than 30 %. The intermediate and hot components are less well constrained. In four out of ten solutions the hot component is split into two parts, the lower of which may interfere with the intermediate temperature component (e.g., the best-fit solution of Fig. 7 does this). Also, in 4 out of the 10 solutions there is a weak, hard component above 5 keV. The effect of this hard component is compensated by lowering the emission measure of the hot component. Therefore, the present data do not allow a detailed breakdown of the hot and intermediate components. Of course, the total emission measure and average temperature of both components combined is well determined. The average total emission measure of the intermediate and hot component (above 0.9 keV) is 7.32 ± 0.08 10^{59} m^{-3}, and all 10 solutions deviate no more than 5 % from this. The emission-measure-averaged temperature of both components is 1.93 ± 0.02 keV, with deviations no larger than 7 %.

4.3.5. Multi-temperature plasma with finite temperature width

In order to investigate whether the three dominant temperature components as found from our three-temperature fit are narrow or broad in temperature width, we have made a model for a multi-temperature plasma where each component i has a Gaussian distribution in (logarithmic) temperature space, i.e.
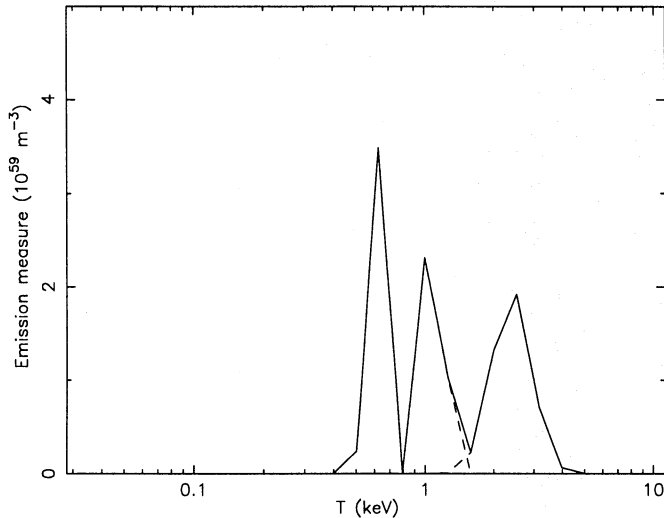
Fig. 8. Emission measure distribution (solid line) of AR Lac using 3 Gaussian temperature distributions. dashed lines: contributions of the 3 individual components

$$Y_i(T) = \frac{Y_i}{\sqrt{2\pi}\sigma_i}e^{-(\log(T) - \log(T_i))^2/2\sigma_i^2} \qquad (6)$$

where Y_i is the total emission measure of the component, T_i its temperature centroid and σ_i the standard deviation.

For three components, we find best-fit temperatures and emission measures that are entirely consistent with our three-temperature fit of Sect. 4.2. All components show a small but not very significant broadening: σ =0.02 (-0.02,+0.08), σ =0.03 (-0.03,+0.30) and σ =0.08 (-0.08, +0.16) respectively for the cool, intermediate and hot component. In Fig. 8 we plot the corresponding emission measure distribution, at the same resolution as for the other methods. It is evident that the cool component is rather narrow; its relative FWHM is not larger than 50 %. Again, the width and structure in the intermediate and hot components are less well constrained. They might span typically a width of a factor of two in temperature.

5. Discussion

5.1. Temperature structure

From our analysis it appears that AR Lac has a bimodal temperature structure: a cool component at 0.6 keV, and an intermediate / hot component with possible substructure near 1 and 2.4 keV. There is no significant emission at temperatures below 0.3 keV. This is confirmed by all our analysis methods.

The cool component is a relatively narrow feature, as our analyses with, in particular, the genetic algorithm and the broadened multi-temperature plasma model shows. It has a relative width not larger than 50 %; smaller widths cannot be resolved with the present observations.

The structures of the hot and intermediate component are less well defined; they constitute certainly not a single, narrow and discrete temperature structure. But as the result of our genetic algorithm shows, there are many different solutions with
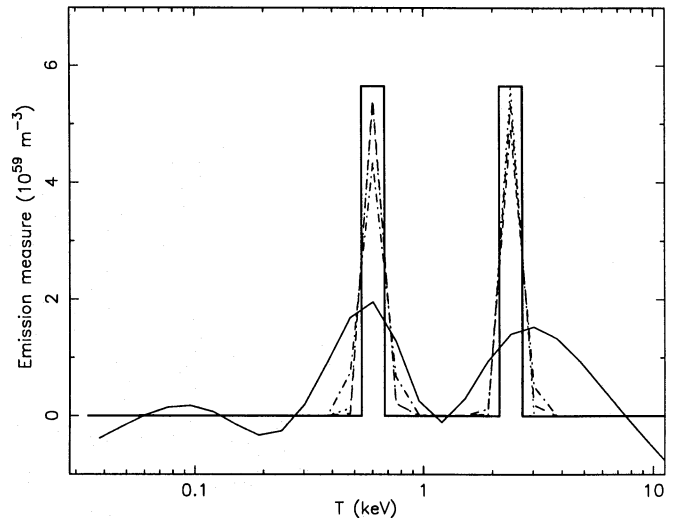

Fig. 9. Reconstructed emission measure distribution for two delta-functions in temperature. Thick solid line: the input model (the sum of two delta-functions, plotted here for clarity as histograms with a width equal to the temperature bin size used); thin solid line: regularisation method; dot-dashed line: polynomial method; dashed line: genetic algorithm; dotted line: two broadened Gaussian components

acceptable χ^2 values. The intermediate and hot component may be two discrete structures, but it is also possible that they originate from the same region, and that they are part of an extended temperature structure spanning the temperature range from below 1 keV up to about 3–4 keV. There might be a weak hard tail above 5 keV extending towards high temperatures, but its presence is not certain; in any case its strength is not larger than 5 % of the total emission measure.

Recently, Walter (1996) published the emission measure distribution obtained from EUVE observations of AR Lac, utilising the polynomial method. His solution also shows a bimodal temperature distribution, which is very similar to our solution with the polynomial method. The peak temperatures in the EUVE spectrum are around 0.5 and 2 keV, similar to our two-temperature fit.

Some readers might ask whether the bimodel structure could be an artifact of the detectors and their sensitivities to various line emissivities. To demonstrate that this is not the case, we have done two simulations.

First, we simulated a two-component spectrum with temperatures of 0.6 and 2.4 keV (the dominant temperatures in our three temperature model), and equal emission measures of $5.65\ 10^{59}$ m^{-3}. Their sum is equal to the total emission measure for the three components of table 1. The emission measure distribution is thus the sum of two delta-functions in the temperature. We have used exactly the same abundances, integration time, response matrices and data selection as used in our present analysis of the AR Lac spectrum. We applied the polynomial, regularisation, genetic and broadened Gaussian component methods to the simulated spectrum. The results are shown in Fig. 9. The regularisation methods smooths the two components somewhat, but is still capable of reconstructing the
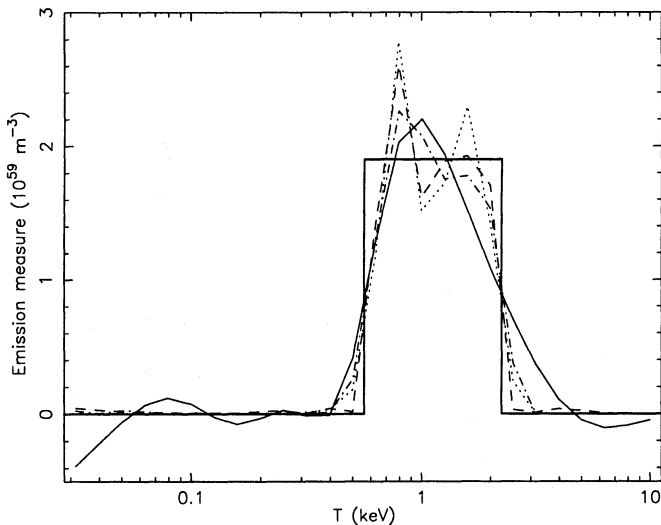
Fig. 10. Reconstructed emission measure distribution for a block profile. Thick solid line: the input model; thin solid line: regularisation method; dot-dashed line: polynomial method; dashed line: genetic algorithm; dotted line: two broadened Gaussian components

bimodal distribution. All other methods essentially reproduce the two sharp discrete structures.

Alternatively, we have used a block function with constant emission measure per bin between 0.6 and 2.4 keV. The total emission measure is also equal to $11.3\ 10^{59}\ \mathrm{m}^{-3}$, with all other conditions similar to the previous simulation. The results are shown in Fig. 10. Again, the regularisation method smoothes the temperature distribution somewhat, but it clearly finds a single, broadened component. The other methods reconstruct the block function reasonably well. The polynomial method does not give a perfect fit, mainly because it is not possible to represent a block function as the sum of less than ~8 Chebyshev polynomes with more accuracy than shown here. The genetic algorithm shows some substructure with amplitudes of the order of 20–30 %; however, doing more simulation runs with different random seeds shows that these substructures always appear at different temperatures, but within the boundaries of the block profile and preserving the global shape of the block profile. In summary, all four methods reproduce essentially the broadened temperature distribution of the block profile. Note that in this and the previous simulations, the best-fit χ^2 values differ by no more than 2. This shows that it is impossible to discriminate between the solutions obtained by the different methods without using any other information.

We conclude that our methods are able to distinguish between a bimodal temperature distribution and a single broadened temperature profile and that the latter type of distribution is inconsistent with the observed soft X-ray spectrum of AR Lac.

5.2. Emission measure analysis methods

We have compared in this paper different emission measure analysis methods. The discrete multi-temperature model with

e.g., two or three temperature components is efficient in deriving the abundances in the dominant temperature components. The temperatures derived must, however, be interpreted with care. We can illustrate this also as follows. We made a simulation of the hot component of AR Lac only, but split it into two components with emission measure $3\ 10^{59}\ \mathrm{m}^{-3}$ each, and temperatures of 1.6 and 2.4 keV. A fit with a two-temperature model gives a χ^2 that is only 5.7 better than a single temperature fit. The best-fit temperature of the single-temperature model, 1.90 ± 0.02 is, although close to the average temperature, still 5σ away from it. On the other hand, the statistical errors on the temperatures in the two-temperature fit are much larger: e.g., 1.51 ± 0.40 for the 1.6 keV component.

The corresponding emission measures give a good indication of the total emission measure in the region of temperature space in which the temperature component is located. The emission measures derived from our three-temperature fit are in good agreement with the emission measures derived from continuous emission models.

Of the continuous emission measure analysis methods used here, both the regularisation method and the Chebyshev polynomial method are able to resolve at least the cool and hot components (Figs. 2 and 3). With sufficient resolution (i.e., sufficiently large number of terms and small temperature range), the polynomial method can also resolve the intermediate and hot components (Fig. 4). In the present case, the clean method fails to converge because the spectrum of the intermediate component cannot be distinguished from a linear combination of the cool and hot components.

The genetic algorithm has the disadvantage that it is very cpu-time consuming. However, it leads to consistent results with the other methods, and it is the only method capable of showing the wealth of solutions that are all acceptable in a statistical sense.

Finally, we note that both the regularisation method and genetic algorithm produce some measure of the uncertainty in the derived temperature distribution for a given temperature. As the referee pointed out, for the other methods, a bootstrap-like method could be used in order to derive the uncertainties in the temperature distribution.

5.3. Abundances

Our present analysis essentially confirms the results of White et al. (1994) and Singh et al. (1996) that the abundances in AR Lac are non-solar, although the precise values are slightly different, due to differences in the analysis method and plasma code used. The abundances of most elements are consistent with 1/3 solar, except for Ne and Ni. This becomes more apparent if we express the abundances in the units of Grevesse et al. (1992). This makes the abundances of N, O, Ne, Ar and Fe 20, 15, 3, 10 and 44 % higher, respectively as compared to Anders & Grevesse (1989). The corresponding abundances of our three-temperature fit are shown in Table 3. The low abundances are yet to be explained. For Ni, one could argue that both the ionisation balance and the line calculations of the Ni-L complex have not been improved
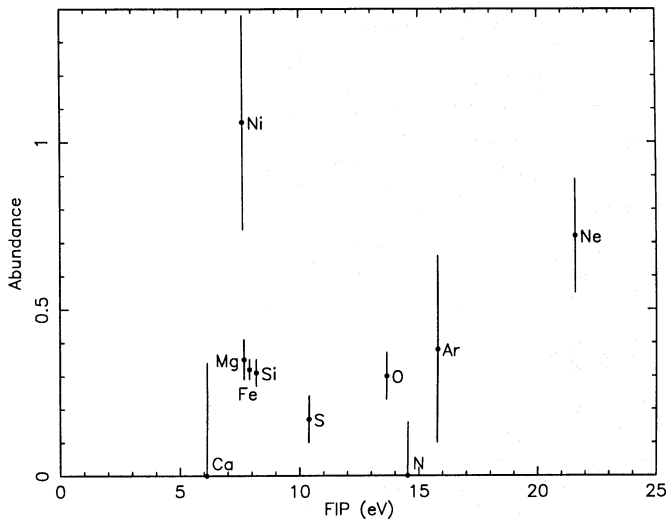
Fig. 11. Elemental abundances of AR Lac in units of the solar photospheric abundances of Grevesse et al. (1992) versus first ionisation potential (FIP)

Table 3. Abundances scaled to Grevesse et al. (1992)

N	O	Ne	Mg	Si	S	Ar	Ca	Fe	Ni
<.16	0.30	0.72	0.35	0.31	0.17	0.38	<.34	0.32	1.06

in our plasma code as compared to what has been done for Fe, but we expect that this could reduce the Ni abundance at most by about 30 %. However the Ni-L complex occurs between 0.8–1.5 keV, and its strength (using the current set of abundances) is about 10–20 % of the strength of the Fe-L complex. Therefore, remaining uncertainties in the Fe-L complex of the order of 5–10 % could reduce (or increase) the deduced Ni-abundance by 50 %. The strongest Ne lines near 1 keV are of comparable strength to the surrounding Fe-L complex. Thus we think that the Ne abundance is higher than for the other elements.

The data show no evidence for a dependence of abundance on first ionisation potential (FIP), as Fig. 11 demonstrates. In the solar corona, elements with low FIP are enhanced with respect to the photospheric abundance (e.g., Meyer 1985, 1990).

An important difference with the analysis of SWD is the use of an updated plasma code. Comparison of the two-temperature fits (Table 1) shows that as a consequence of both the different ionisation balance and the use of the newer Fe-L calculations, the abundance of Fe decreased by 35 %. This is much larger than the statistical accuracy of 10 % in the Fe abundance. Therefore, for a good determination of the Fe abundance (and also for the correlated Ne and Ni abundances) it is essential to use the most recent plasma code.

The ASCA SIS and GIS and the ROSAT PSPC are not sensitive enough to detect significant abundance differences among the various spectral components. For the hot component, we cannot exclude an abundance that is twice as high as the cool and intermediate components. Such abundances for the hot component are, however, still significantly below the solar abundances.

References

Anders E., Grevesse N., 1989, Geochim. Cosmochim. Acta 53, 197
Arnaud M., Raymond J., 1992, ApJ 398, 394
Arnaud M., Rothenflug R., 1985, A&AS 60, 425
Charbonneau P., 1995, ApJS 101, 309
Drake S.A., Singh K.P., White N.E., Simon T., 1994, ApJ 436, L87
Drake S.A., Singh K.P., White N.E., 1996, in: IAU Coll. 152, Astrophysics in the Extreme Ultraviolet, p. 147, Bowyer S., Malina R.F. (eds.), Kluwer.
Grevesse N., Noels A., Sauval A.J., 1992, in: Proc. first SOHO workshop, ESA SP-348, 305
Harrison, R.A., Thompson, A.M., 1992, Rutherford Appleton Laboratory report RAL-91-092
Högbom J.A. 1974, A&AS 15, 417
Kaastra J.S., Mewe R., 1993, Legacy 3, 16
Kaastra J.S., Mewe R., Nieuwenhuijzen H., 1995, in: The 11th coll. on UV and X-ray spectrosc. of astrophys. and lab. plasmas, Watanabe T. (ed.). In press.
Lemen J.R., Mewe R., Schrijver C.J., Fludra A., 1989, ApJ 341, 474
Liedahl D.A., Osterheld A.L., Goldstein W.H., 1995, ApJ 438, L115
Mewe R., Gronenschild E.H.B.M., van den Oord G.H.J., 1985, A&AS 62, 197
Mewe R., Lemen J.R., van den Oord G.H.J., 1986, A&AS 65, 511
Mewe R., Kaastra J.S., Schrijver C.J., van den Oord G.H.J., 1995a, A&A 296, 477
Mewe R., Kaastra J.S., Liedahl D.A., 1995b, Legacy 6, 16
Mewe R., Kaastra J.S., White S.M., Pallavicini R., 1996, submitted to A&A
Meyer, J.-P., 1985, ApJS 57, 151
Meyer, J.-P., 1990, Adv. Space Res. 11, 269
Morrison R., McCammon D., 1983, ApJ 270, 119
Rucinski S.M., Mewe R., Kaastra J.S., Vilhu O., White S.M., 1995, ApJ 449, 900
Schmitt J.H.M.M., Drake J.J., Stern R.A., 1996, submitted to ApJ
Schrijver C.J., Mewe R., van den Oord G.H.J., Kaastra J.S., 1995, A&A 302, 438
Schrijver C.J., van den Oord G.H.J., Mewe R., 1994, A&A 289, L23
Singh K.P., White N.E., Drake S.A., 1996, ApJ 456, 766 (SWD)
Stern R.A., Lemen J.R., Schmitt J.H.M.M., Pye J.P., 1995, ApJ 444, 45
Walter, F.M., 1996, in: IAU Coll. 152, Astrophysics in the Extreme Ultraviolet, p. 129, Bowyer S., Malina R.F. (eds.), Kluwer.
White N.E., 1996, in: 9th Cambridge workshop on cool stars, stellar systems, and the sun, Pallavicini R., Dupree A.K. (eds.). In press.
White N.E., Arnaud K.A., Day C.S.R. et al., 1994, PASJ 46, L97